THE JOURNAL OF BIOLOGICAL CHEMISTRY VOL. 283, NO. 15, pp. 9805–9813, April 11, 2008

Alanine Scanning Mutagenesis of the Prototypic Cyclotide Reveals a Cluster of Residues Essential for Bioactivity*[S]

Received for publication, November 13, 2007, and in revised form, January 11, 2008 Published, JBC Papers in Press, February 7, 2008, DOI 10.1074/jbc.M709303200

Shane M. Simonsen[1], Lillian Sando, K. Johan Rosengren, Conan K. Wang, Michelle L. Colgrave, Norelle L. Daly[2], and David J. Craik[3]

From the Institute for Molecular Bioscience, University of Queensland, St. Lucia, Brisbane, Queensland 4072, Australia

The cyclotides are stable plant-derived mini-proteins with a topologically circular peptide backbone and a knotted arrangement of three disulfide bonds that form a cyclic cystine knot structural framework. They display a wide range of pharmaceutically important bioactivities, but their natural function is in plant defense as insecticidal agents. To determine the influence of individual residues on structure and activity in the prototypic cyclotide kalata B1, all 23 non-cysteine residues were successively replaced with alanine. The structure was generally tolerant of modification, indicating that the framework is a viable candidate for the stabilization of bioactive peptide epitopes. Remarkably, insecticidal and hemolytic activities were both dependent on a common, well defined cluster of hydrophilic residues on one face of the cyclotide. Interestingly, this cluster is separate from the membrane binding face of the cyclotides. Overall, the mutagenesis data provide an important insight into cyclotide biological activity and suggest that specific self-association, in combination with membrane binding mediates cyclotide bioactivities.

Cyclotides are a fascinating family of plant-derived mini-proteins of around 30 residues that are characterized by the topologically unique combination of a head-to-tail cyclized backbone and a cystine knot. The original discovery of the prototypic member kalata B1 (1) was guided by the indigenous medicinal use in Africa of a tea made from the plant *Oldenlandia affinis* (Rubiaceae) to accelerate childbirth. Kalata B1 was identified as a uterotonic component of the plant, but its unusual macrocyclic nature (2) and the fact that it was just one member of a large family of related macrocyclic peptides were elucidated only recently (3). Cyclotides have now been reported in several other species of the Rubiaceae (coffee) family (4, 5) and in all tested members of the Violaceae (violet) plant family (3, 6, 7) bringing the number of known cyclotides to over 100. Individual plants contain a suite of dozens of cyclotides, and analyses of crude plant extracts have suggested that thousands more cyclotide sequences await discovery (8, 9), potentially making them one of the largest known families of plant proteins. Other examples of head-to-tail cyclized proteins have recently also been reported in bacteria, plants, and animals (10, 11).

Cyclotides display a wide range of biological activities. In addition to their uterotonic activity (12), hemolytic (6), anti-HIV[4] (13), anti-bacterial (14), anti-tumor (15), anti-fouling (16), and insecticidal (17) activities have been reported. The mechanism(s) of action of these activities are unknown but may involve interactions with membranes (18, 19), possibly via self-association of cyclotides to form multimeric species (20). Reported structures of cyclotides show the presence of a surface-exposed hydrophobic patch (2, 21) that may be involved in such interactions. Their natural function in plants appears to be as host defense agents against insect pests based on their potent inhibition of growth and development of caterpillar larvae of the cotton budworm and cotton bollworm (17, 22).

Fig. 1 shows the three-dimensional structure and amino acid sequence of kalata B1 and highlights the knotted arrangement of the three conserved disulfide bonds that are characteristic of all cyclotides. The cystine knot and cyclic backbone account for the exceptional resistance of the cyclotides to thermal, chemical, and enzymatic degradation compared with other peptides of similar size (23). This chemical and biological resilience has led to suggestions of the use of cyclotides as protein-engineering scaffolds for stabilizing bioactive peptide epitopes in the optimization of peptide drugs (24–27).

The sequences of currently known cyclotides reveal subsets of conserved and variable residues. In describing cyclotides it is convenient to discuss their structures in terms of the six backbone loops between successive cysteine residues. The cyclotides may be regarded as a natural combinatorial template in which substitutions occur in these loops, which protrude from the cystine knot core (Fig. 1). Loop 1 is the most highly conserved and contains a structurally important glutamate residue that forms a network of hydrogen bonds to the backbone of the first two residues of loop 3 (28). Cyclotide sequences have been divided into the Möbius and bracelet subclasses (3), which differ from one another mostly in loops 2, 3, and 5, but the characteristic discriminating feature is a *cis*-Pro peptide bond in loop 5 of the Möbius subfamily, so named for its conceptual 180° twist of the circular backbone.

* This work was supported in part by a grant from the Australian Research Council (ARC). The costs of publication of this article were defrayed in part by the payment of page charges. This article must therefore be hereby marked "*advertisement*" in accordance with 18 U.S.C. Section 1734 solely to indicate this fact.

[S] The on-line version of this article (available at http://www.jbc.org) contains supplemental Fig. S1.

[1] Supported by an Australian Postgraduate award.

[2] An National Health and Medical Research Council Industry Fellow.

[3] An ARC Professorial Fellow. To whom correspondence should be addressed: Tel.: 61-7-3346-2019; Fax: 61-7-3346-2029; E-mail: d.craik@imb.uq.edu.au.

[4] The abbreviations used are: HIV, human immunodeficiency virus; HPLC, high-performance liquid chromatography; kB1, kalata B1; E7A, [E7A]-kalata B1; T27A, [T27A]-kalata B1.

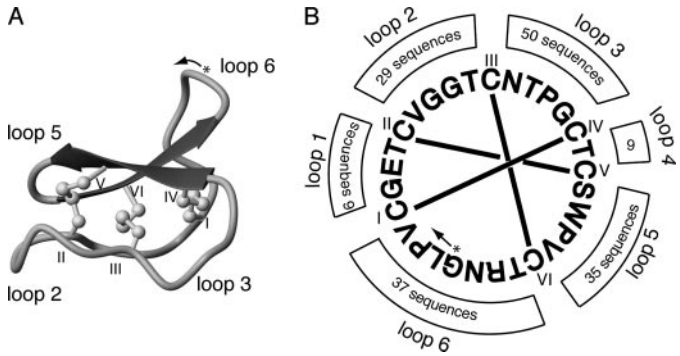

FIGURE 1. **The structure of the prototypic cyclotide kalata B1.** *A*, the three-dimensional structure of kalata B1 is shown in *ribbon format*, with the *arrows* representing the β-strands and the disulfide bonds shown in *ball-and-stick format*. The cysteine residues are labeled with *Roman numerals*. *B*, the sequence of kalata B1 with the disulfide bonds is shown as *lines* connecting the cysteine residues. The number of different sequences for known cyclotides for each loop is shown *outside the sequence*.

Investigation of the contribution of individual residues to the structural integrity and biological activities of the cyclotides is crucial to facilitate their use in protein engineering or pharmaceutical applications. A clearer understanding of the structural limitations of the cyclotide framework will greatly assist in developing grafted analogues for use as peptide drugs so that sequence modifications in structurally important regions can be avoided. Understanding the basis for bioactivity will also allow undesirable properties such as hemolytic activity to be minimized in pharmaceutical applications.

A better appreciation of the structure-activity relationships of the cyclotides also has the potential to help uncover the mechanism(s) mediating their various bioactivities. Hence, in the current study we chemically synthesized a complete suite of kalata B1 mutants, in which all residues, except for the six conserved cysteines, were individually replaced with an alanine. We analyzed these alanine mutants for structural and functional perturbations relative to native kalata B1 and determined their activities against insects and human cells. This approach has provided significant insights into the structural constraints of the cyclotide framework and the functional elements for bioactivity and has provided a more detailed understanding of the possible self-association process of these remarkable peptides.

EXPERIMENTAL PROCEDURES

Peptide Synthesis—*t*-Butoxycarbonyl-based solid phase peptide synthesis was carried out using standard protocols (29). Peptides were assembled using a thioester linker assembled on resin, allowing subsequent cyclization by a modified form of native chemical ligation (30). Synthesis was structured into batches starting at V4, T8, T13, G18, and V25 that allowed bulk assembly of the native peptide sequence then the resin was split for assembly of individual alanine mutants in the terminal loops. Hydrogen fluoride cleavage was conducted on the deprotected resins following standard protocols (0 °C, 90 min, 90% hydrogen fluoride/8% *p*-cresol/2% *p*-thiocresol). Crude cleavage products were purified by reversed phase C_{18} HPLC (1%/min gradient of 90% acetonitrile/10% water/0.05% trifluoroacetic acid against 100% water/0.05% trifluoroacetic acid) to give linear, reduced, C-terminally thioester-capped peptides. Peptides were cyclized and oxidized in 0.1 M ammonium bicarbonate at pH 8 containing 50% 2-propanol overnight and purified as above. Purity of fractions was assessed using electrospray ionization-mass spectrometry and analytical HPLC using a 2%/min gradient of the same solvents used for previous steps.

NMR Spectroscopy—NMR solutions for assignment and structure determination were prepared in H_2O:D_2O (95:5) and adjusted to pH 5.0–5.5 (or 3.0–3.5 for mutant E7A) with 0.1 M NaOH and 0.1 M HCl. Samples for amide temperature coefficients were prepared in 100 mM sodium phosphate buffered at pH 5.5 with 5% D_2O adjusted to pH 5.0–5.5 (or 3.0–3.5 for mutant E7A). Chemical shifts and amide temperature coefficients for mutant E7A were compared with the wild-type peptide under similar conditions. One- and two-dimensional spectra were acquired on ARX 500-MHz or 600-MHz spectrometers at 25 °C.

Structure Calculations—Preliminary structures were calculated using a torsion angle-simulated annealing protocol within the program DYANA (31). Final structures were calculated using simulated annealing and energy minimization protocols within CNS version 1.1 (32). The starting structures were generated using random (ϕ, ψ) dihedral angles and energy-minimized to produce structures with the correct local geometry. A set of 50 structures was generated by a torsion angle-simulated annealing protocol (33, 34). Structures consistent with restraints were subjected to further molecular dynamics and energy minimization in a water shell, as described by Linge and Nilges (35). Structures were analyzed using PROMOTIF (36) and PROCHECK-NMR (37). The Ramachandran statistics for E7A are 75.8% of residues in the most favored and 24.2% in the additionally allowed. For T27A the Ramachandran statistics are 87.4% in the most favored and 12.6% in the additionally allowed.

Hemolytic Assays—Stock solutions of each peptide were prepared and standardized using UV spectroscopy (ϵ = 6410 cm^{-1-1} at 215 nm) at 350 μM ± 3% then serially diluted in triplicate. Human erythrocytes were washed with repeated centrifugation in phosphate-buffered saline (pH 7.4) to remove serum contaminants. A 0.25% v/v stock solution was prepared from the cell pellet, and 100 μl of this stock was added to each diluted peptide solution aliquot and then incubated at 37 °C for 1 h. After centrifugation of intact cells the percentage of hemolysis of the supernatant was measured by visual absorption spectroscopy (λ = 405 nm).

Insecticidal Assays—Adult *Drosophila melanogaster* were allowed to oviposit overnight on plates (7 g of agar/7 g of sucrose/260 ml of water/70 ml of apple juice), and the resulting eggs were collected and washed with repeated centrifugation. The volume of eggs for each trial could only be approximated to within ± 50 μl, so the wild-type peptide was included in each batch of assays on alanine mutants as a reference positive control. The egg pellet was diluted with 50% glycerol and aliquoted into vials containing 3 ml of basic larval media (10 g of agar/80 g of cornmeal/200 g of yeast/850 ml of water/100 ml of treacle/11 ml of 10% w/v nipogen/5 ml of propionic acid). Glycerol was added to increase the viscosity to assist in homogeneous dispersion of eggs throughout the suspension. After 24-h incubation test compounds were added as UV absorption standardized solutions to give final peptide concentrations of 230, 100,

or 0 ppm (or 80, 35, and 0 μM, respectively). Larvae were then allowed to mature and pupate, and the mass of total flies emerging was measured over 2–3 days.

Stability Assays—Enzymatic digests and acid hydrolysis conditions were identical to those described previously (23). Briefly, 1 mg/ml solutions of WT-kB1, G6A, or E7A were prepared in 100 mM ammonium bicarbonate buffer (pH 8.1). The enzymes used in these studies were trypsin, chymotrypsin, and proteinase K. Enzymatic digestions (50:1 substrate-to-enzyme ratio) were carried out at 37 °C with aliquots taken at set times up to 24 h. DnaK fragment 2 was used as a control to ensure that the enzymes were active. With this control, and because we were primarily interested in quantifying short term degradation, if present, no corrections for autodigestion of the enzymes were required. Acid hydrolysis reactions (1 mg/ml peptide solution in 1 M HCl) were performed at two temperatures, 37 °C and 80 °C. Samples were analyzed by liquid chromatography/mass spectrometry on an Agilent Series 1100 HPLC coupled to a QSTAR mass spectrometer (Applied Biosystems, Foster City, CA) equipped with an electrospray ionization source. Data were collected, processed, and analyzed using the Analyst QS1.1 software package. Thermal stability was assessed by monitoring the quality of one-dimensional NMR spectra of compounds in water at pH 5.0–5.5 for G6A and 3.0–3.5 for E7A on cycling from 25 °C to 80 °C and back to 25 °C.

Metal Binding—Titration of 0.4 mM kalata B1, T27A, T16A, and E7A with $MnCl_2$ was performed at 40 °C, pH 5.0. One-dimensional and total correlation spectroscopy spectra (80-ms mixing time) were acquired at concentrations of 0 and 2.0 mM $MnCl_2$ on an ARX 500-MHz spectrometer. The paramagnetic relaxation enhancement induced by Mn^{2+} was qualitatively characterized by relative cross-peak intensity in the total correlation spectroscopy spectra,

$$RCI_i = 100\%(I_i^{Mn^{2+}}/I_i^0) \quad \text{(Eq. 1)}$$

where I_i^{Mn2+} and I_i^0 are the HN-Hα cross-peak intensities in the spectra of the sample with and without Mn^{2+}.

RESULTS

Synthesis—Kalata B1, the prototypic cyclotide, comprises 29 amino acids, including 6 cysteine residues. This alanine mutagenesis study therefore required the synthesis of 23 individual peptides, which was achieved by *t*-butoxycarbonyl-based solid phase peptide synthesis. The cyclization was achieved using a modified form (14, 38) of native chemical ligation (39) and required that the linear precursor protein had a Cys at the N terminus. For rapid and economical generation of mutants, several large batches of the initial unmodified sequence were synthesized, each from a different starting position. When only a single loop (or two small loops) remained to be synthesized in each batch, the resin was split into aliquots for selective alanine mutagenesis of each residue in the loop(s). After cleavage from the resin and purification, the peptides were cyclized and oxidized at pH 8 in a 1:1 ammonium bicarbonate:2-propanol buffer. Yields of the alanine mutants were in many cases similar to the native peptide and are summarized in Table 1. Notably, variants of loops 2 and 5 gave significantly reduced yields of correctly folded products, and the P24A and W23A mutants of loop 5 did not form the native fold using folding conditions applied for all other analogues. Mutant W23A was subsequently found to form a native fold upon addition of 1 mM glutathione to the folding buffer. However, it was not assayed with the other analogues. The decision to omit glutathione from the original folding buffer was made to simplify the conditions, rather than to optimize yield, and it is likely that increased yields of individual mutants can be achieved after optimization of the conditions.

TABLE 1
Yields of folded Ala-mutant cyclotides and hemolytic and insecticidal activity

Mutant	Yield[a]	Hemolytic activity[b]	Insecticidal activity[c]
		%	
WT	100	69	100
G1A	50	68	102
L2A	71	12	100
P3A	7	37	31
V4A	82	34	115
G6A	54	1	2
E7A	46	1	0
T8A	64	8	15
V10A	21	49	108
G11A	25	61	91
G12A	11	11	31
T13A	25	46	118
N15A	68	4	68
T16A	100	5	55
P17A	50	49	83
G18A	79	62	119
T20A	64	62	131
S22A	36	59	118
W23A	0		
P24A	0		
V25A	21	9	133
T27A	68	69	119
R28A	68	15	100
N29A	39	54	102

[a] Relative to wild type (WT) at 100%. A typical wild-type kalata B1 oxidative folding yield is 28% under comparable conditions.
[b] Relative to 100% lysis control standard of 10 μl of 1% w/v Triton X-100.
[c] Relative to 100% control of wild-type peptide at 230 ppm (80 μM) peptide (LD_{50} = 150 ppm (52 μM)).

Global Fold of Mutants as Assessed by NMR—The alanine mutants of kalata B1 were dissolved in water and two-dimensional NMR spectra were recorded at pH 5.0–5.5. The α-proton chemical shifts of peptides are sensitive indicators of local structure (40) and were used to highlight regions of perturbed structure. The majority of alanine mutants had no significant α-H chemical shift perturbations compared with the wild-type peptide, as shown in Fig. 2*A*. A small subset of mutants showed some minor localized shift perturbations as shown in Fig. 2*B*. The alanine mutants in loop 2 account for the majority of these slightly perturbed structures. For mutant E7A several expected peaks were missing from the spectra at pH 5.0–5.5 (presumably due to broadening) but were present at pH 3.0–3.5, indicating that this mutant is less able to form a rigid secondary structure at the higher pH. Overall though, the chemical shift analysis showed that generally no major structural changes are induced by Ala substitution at any of the individual non-Cys residues and that the overall cyclotide fold is maintained in all mutants.

Two alanine mutants were selected for full structure determination. Mutant E7A was selected to investigate the effect of removal of the internal hydrogen-bonding network from the glutamate side chain to the backbone amides of loop 3. Mutant

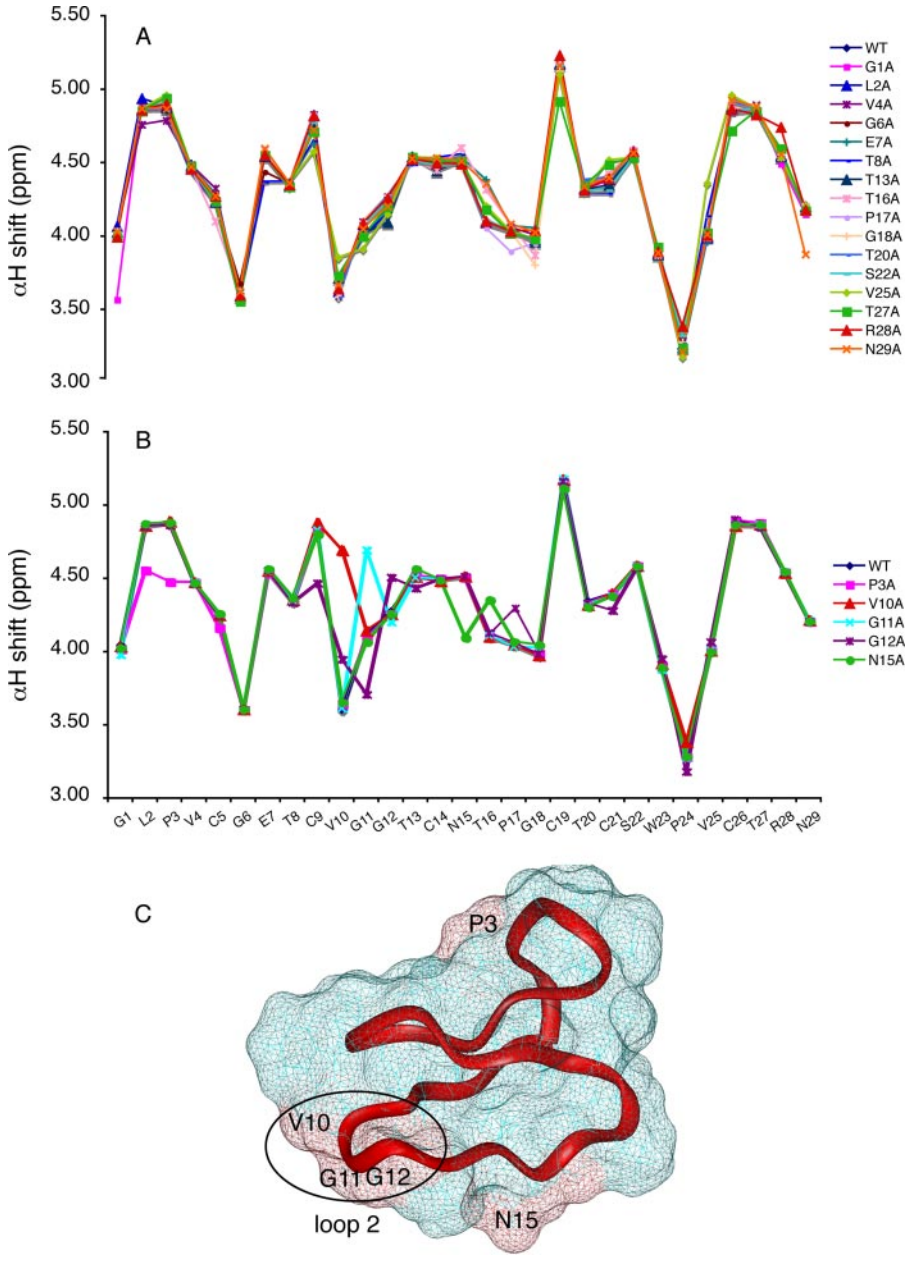

FIGURE 2. **Chemical shift differences of αH signals for kalata B1 alanine mutants compared with the wild-type peptide.** *A*, mutants with minimal chemical shift changes from the wild-type peptide. *B*, mutants with small local chemical shift changes from the wild-type peptide, particularly in loops 2 and 3. *C*, a structure of kalata B1 showing the location of the residues that are most susceptible to chemical shift change on substitution.

T27A was selected as a relatively unperturbed example based on the chemical shift data. The three-dimensional structures of E7A and T27A were solved by simulated annealing using distance and angle restraints derived from two-dimensional NMR spectra. Simulated annealing calculations gave ensembles of 20 low energy structures with backbone root mean square deviations of 0.5 Å for E7A and 0.5 Å for T27A as summarized in Table 2. The structures of E7A and T27A are shown in Fig. 3, and they confirm that the overall fold of the mutants does not substantially differ from the wild-type peptide.

Bioassays—The biological activities of the mutant peptides were assessed in insecticidal and hemolytic assays. The former activity is of interest because of the suggestion that the native activity of cyclotides in plants is for host defense against insects (17, 22), and the latter activity is of interest because it is a potentially deleterious effect should cyclotides be applied in pharmaceutical applications. Insecticidal activity of the alanine mutants was assessed by measuring their impact on the development of first and second instars of *Drosophila melanogaster* to adulthood. This assay consumed ~3 mg per test compound by using triplicates at two peptide concentrations. Triplicates were found to vary by <10%. Wild-type kalata B1 and alanine mutants gave reproducible dose response curves with an approximate LD_{50} of 150 ppm (52 μM) for the wild-type peptide. The mass of emerging adult flies varied inversely with the mass of eggs aliquoted. The activity of the alanine mutants relative to the wild-type peptide is reported in Table 1, where it is clear that substitution of a specific set of individual residues leads to a loss of activity. Thus, despite the fact that no Ala substitution causes a major structural change, there are functional effects of individual residues.

The relative hemolysis of human erythrocytes caused by each mutant is also shown in Table 1, which indicates that residues in loops 1 and 3 along with a few other isolated residues strongly affect activity. Interestingly, a comparison of the results from both bioassays indicates that hemolytic activity and insecticidal activity depend on a similar subset of residues.

Stability Analysis—The stability of the G6A and E7A mutants was assessed by measuring their resistance to proteolysis and to acid hydrolysis. Mass spectra were examined for the presence of intact peptides and/or degradation products, and the percentage of intact peptide remaining was plotted against time. The two alanine mutants studied were completely impervious to enzymatic digestion by the three endoproteinases trypsin, chymotrypsin, and proteinase K, as was the prototypic cyclotide kalata B1. A linear control peptide degraded rapidly, with <5% remaining after 5 min under the same conditions. Acid hydrolysis experiments were conducted at 37 °C and 80 °C. The former represents likely conditions in the human stomach (pH ~ 1, 37 °C), whereas the higher temperature was used to force the hydrolysis to occur and allow comparison of the stability of

the mutants to the wild-type cyclotide. At 37 °C, kalata B1, and the two mutants were extremely stable, with no degradation products observed for up to 24 h. At 80 °C, the peptides degraded within 90 min and showed similar degradation curves from 0–90 min (data not shown).

Thermal stability was assessed by monitoring the one-dimensional NMR spectra of peptides on cycling from 25 °C to 80 °C and back to 25 °C. The spectra of both mutants were unchanged on return to the original temperature, but E7A lost more amide peaks at higher temperature than the wild-type peptide and G6A (data not shown). Overall, the data suggest that the structures of the mutants are highly resistant to extremes of temperature, pH, and enzyme conditions, but the E7A mutant is slightly more susceptible to thermal unfolding and is more flexible.

TABLE 2
Structural statistics for the alanine mutants E7A and T27A of kalata B1

	E7A	T27A
NMR distance and dihedral constraints		
Distance constraints		
Total NOE	261	184
Intra-residue		
Inter-residue	261	184
Sequential ($\|i-j\|=1$)	143	89
Medium range ($\|i-j\|<4$)	49	36
Long-range ($\|i-j\|>5$)	69	59
Intermolecular		
Hydrogen bonds	0	16
Total dihedral angle restraints	13	24
ϕ	9	12
ψ	0	0
Structure statistics		
Violations (mean ± S.D.)		
Distance constraints (Å)	0.023 ± 0.002	0.029 ± 0.002
Dihedral angle constraints (°)	0.155 ± 0.08	0.67 ± 0.1
Max. dihedral angle violation (°)	2.8	2.6
Max. distance constraint violation (Å)	2	2
Deviations from idealized geometry		
Bond lengths (Å)	0.003 ± 0.0001	0.004 ± 0.0002
Bond angles (°)	0.49 ± 0.02	0.55 ± 0.02
Impropers (°)	0.40 ± 0.023	0.42 ± 0.04
Average pairwise root mean square deviation[a] (Å)		
Heavy	0.90 ± 0.2	1.09 ± 0.2
Backbone	0.5 ± 0.2	0.5 ± 0.2

[a] Pairwise root mean square deviation was calculated among 20 refined structures.

Metal Binding—A representative group of mutants was selected and compared with kalata B1 to examine the significance of a putative metal binding site reported previously for kalata B1 (41, 42). The mutants selected were E7A (an inactive mutant without the carboxyl from E7), T16A (an inactive mutant with the carboxyl), and T27A (an active mutant with the carboxyl). A series of total correlation spectroscopy spectra was measured for each peptide in solution with and without Mn^{2+}. In the presence of Mn^{2+} kalata B1, T16A and T27A showed specific broadening of a defined set of amide signals, consistent with previous reports for kalata B1 (41). There was almost complete broadening of the amide signals from C14, N15, and T16/A16, and significant broadening (*i.e.* ~70% attenuation) of loop 1 residues. By contrast, E7A showed significantly less broadening (supplemental Fig. S1). It is clear that removal of the E7 carboxyl group reduces the effects of Mn^{2+}, implicating it as the primary binding site.

DISCUSSION

In this study a complete suite of non-cysteine alanine mutants was chemically synthesized and evaluated for structural and functional perturbations relative to the prototypic cyclotide kalata B1. From this we have gained valuable insights into the structural and functional contributions of specific residues in the cyclotide kalata B1, and the data provide a basis for understanding the mechanism of bioactivity of cyclotides.

Chemical solid phase peptide synthesis was used to generate the 23 non-cysteine alanine mutants. Backbone cyclization was achieved using a modified form of native chemical ligation in which the linear peptide is synthesized with a C-terminal thioester that is repeatedly exchanged with cysteine thiol side chains, culminating in the N-terminal cysteine thiol that undergoes an irreversible exchange with the N-terminal amine to form the linking backbone amide (43). Exploitation of this mechanism permitted designing the synthesis with any linear precursor that terminated in an N-terminal cysteine. This allowed the synthesis of the alanine mutants to start at multiple different positions in the sequence, allowing the resin from a bulk synthesis of unmodified cyclotide sequence to be split at the appropriate point in the chain assembly process to produce a set of alanine mutants from the final loop(s).

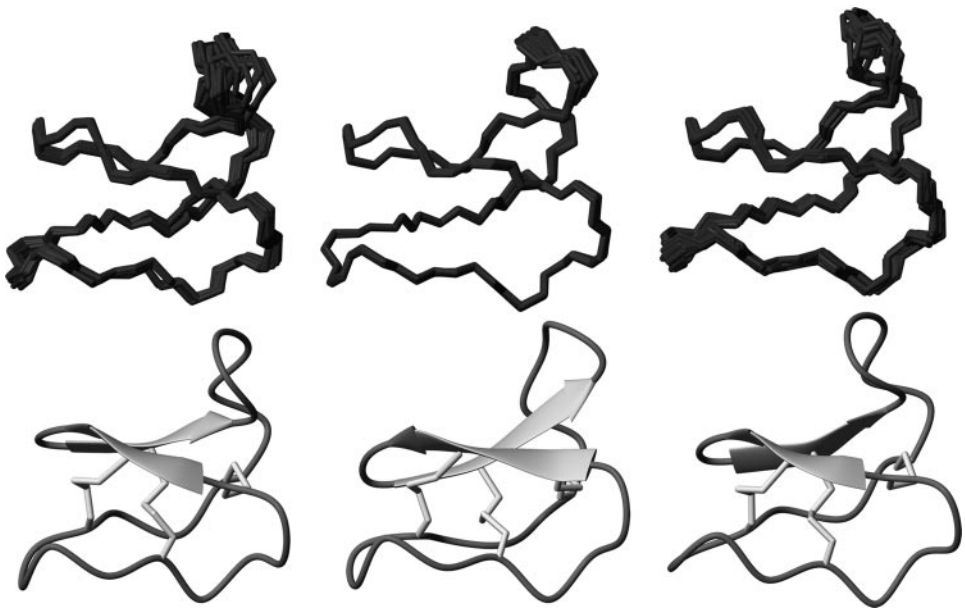

FIGURE 3. **Structure of alanine mutants and wild-type kalata B1.** *Left*: three-dimensional structures of [E7A]-kB1 determined using NMR spectroscopy. The 20 lowest energy structures are presented. *Center*: wild-type kalata B1 (PDB code 1NB1). *Right*: mutant [T27A]-kB1. The disulfide bonds are shown in *stick format* and the β-strands as *arrows*.

The mutants were cyclized and subjected to oxidative folding in ammonium bicarbonate/2-propanol buffer, with the yields summa-

rized in Table 1. All of the mutants formed a native fold in this buffer, with the exception of W23A and P24A, which involve substitutions in loop 5. There was a variation in yield of the correctly folded product relative to the wild-type peptide; peptides with lower yields had mutations primarily concentrated in loops 2 and 5, along with an isolated example of P3A in loop 6 having a low yield. The tight turns of loops 2 and 5 and their close packing in the structure of the native peptide explain the sensitivity of these regions to modification. Mutant G12A had a particularly low yield that is likely associated with its broadened chromatographic peaks during purification, suggesting that this mutant may be conformationally flexible. Introduction of a side chain at this position appears to disfavor the positive ϕ-angle present for this highly conserved glycine that is present in almost half of known cyclotide sequences (44).

The chemical shifts of the α-protons of the alanine mutants relative to the wild-type peptide gave useful insights into the structural resilience of the cyclotide framework. The majority of mutants had no significant perturbations in shift, showing that the framework is highly tolerant to point substitutions. A small subset of mutants experienced minor local shift perturbations in the modified region (Fig. 2*B*) generally in mutants that also displayed lowered oxidative folding yields. The most significant changes in chemical shifts occurred in loop 2, with loops 5 and 6 displaying the lowest variation in shifts. Combined with the folding yield observations this finding indicates that future sequence modification attempts may be more successful if they concentrate on loops 3 or 6. Loop 3 represents the most diverse loop in terms of length in native cyclotide sequences and is extended into a short 3^{10} helix in the bracelet cyclotides (28).

The glutamic acid in loop 1 is almost completely conserved in the cyclotides, only conservatively sub-

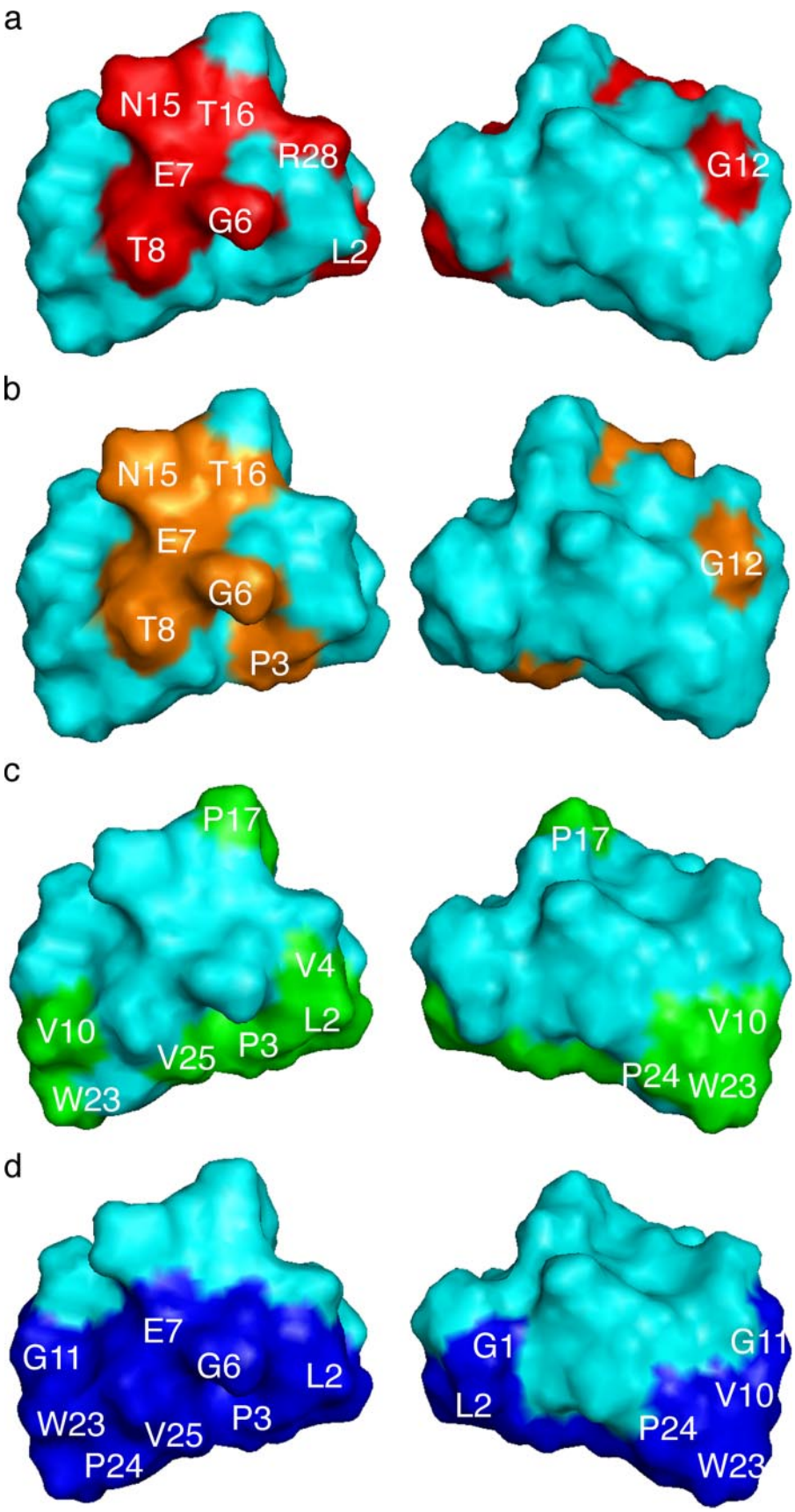

stituted with aspartic acid in one known sequence (45), and is involved in a network of hydrogen bonds that stabilize the structure (28). Analysis of the NMR structure of mutant E7A was initially hindered by the poor spectra and an atypical pH sensitivity of this compound. Numerous amide resonances were not detected at pH ~5.5, indicating that this mutant undergoes a conformational exchange process not seen in the wild-type peptide. These resonances were more readily detected at lower pH, and the structure determined at pH 3.5 is shown in Fig. 3 (*left structures*). Despite the loss of the network of hydrogen bonds involving E7 the overall fold of E7A is maintained. Thus, the most significant structural effects of mutation of this conserved Glu are related to an increased flexibility of the structure at higher pH. This effect is similar to the loss of stability previously seen in acyclic permutants of kalata B1 (46, 47). The importance of the glutamic acid residue has also been recently highlighted by the observation that methylation of this side chain resulted in a 48-fold decrease in cytotoxicity activity for the bracelet cyclotide cycloviolacin O2 (48). This finding confirms the critical importance of this residue in both subfamilies of cyclotides. The structure of mutant T27A, determined as an example of a mutant that retained its bioactivity, showed no significant difference to the wild-type peptide structure, as shown in Fig. 3 (*right structures*). This finding supports the use of chemical shifts as a marker for a lack of structural change for the other mutants also.

Superimposition of the bioassay results onto the structure of the prototypic cyclotide highlights the stunning result that all of the residues responsible for either insecticidal or hemolytic activity are tightly clustered on a patch on one face of the molecule. As indicated in Fig. 4, most of the critical residues are located in loop 1, and to a lesser degree at the beginning of loop 3, and the cationic Arg-28. The single exception is G12A, and, as noted earlier, this is associated with a degree of conformational flexibility of this mutant, as judged by substantially broadened HPLC peaks. The localization of residues responsible for activity in such a defined patch suggests that this patch is associated with a crucial binding interaction. In general such an interaction could be with a receptor, a membrane, or a cognate binding protein. Because cyclotides have been demonstrated to bind to membranes we first explored the possibility that the bioactive patch is implicated in membrane binding.

We were at first very surprised to see that the surface-exposed hydrophobic patch of kalata B1 shown in Fig. 4*c* is clearly distinct from the residues that are crucial for bioactivity. Spin label studies recently demonstrated that this surface-exposed hydrophobic patch essentially forms the membrane binding face of the cyclotide kalata B1, as shown in Fig. 4*d* (42). This finding, together with the mutagenesis results from this work clearly suggests that more than simple membrane interactions must mediate bioactivity. The high level of sensitivity of bioactivity to changes in hydrophilic rather than hydrophobic residues indicates that the activity of kalata B1 is not dependent on gross physical characteristics and that the peptide does not act as a simple detergent. This extreme sensitivity of activity to loss of hydrophilic residues (*e.g.* T8A) or to small steric changes (*e.g.* G6A) and the clustering of critical residues instead indicate that a specific recognition process takes place that does not directly involve the membrane binding face.

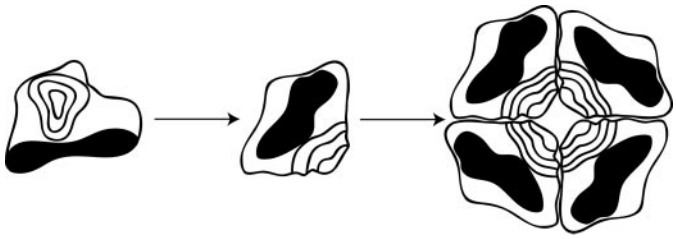

FIGURE 5. **Schematic representation of proposed tetramer model of kalata B1.** The *shaded regions* represent the hydrophobic surface patch known to be associated with membrane binding, and the *contoured regions* represent the hydrophilic face that is correlated with bioactivity. It is proposed that mutation of these residues reduces the propensity for self-association and thereby indirectly leads to reduced membrane binding and activity.

This recognition process could in principle be mediated via a cellular receptor that is common to the many biological processes (including hemolysis, insecticide activity, and anti-HIV activity) that are sensitive to cyclotides, by self-recognition, or by a combination of both. The very wide range of biological activities of the cyclotides and consistent bioactivity across substantial cyclotide sequence variations are more consistent with a non-receptor-based mechanism and suggests that self-association is an integral part of their biological activity. Self-association is well established in other membrane-disrupting peptides (49, 50). Studies using analytical ultracentrifugation (20) indicate that kalata B2 (and to a lesser degree kalata B1) self-associate in sodium phosphate buffer to form tetramers and octamers. The lack of any observable dimers or trimers indicates that cyclotides are capable of a specific oligomerization process. We suggest here that this specific oligomerization, along with subsequent membrane binding, is vital for cyclotide bioactivity.

The hydrophobic and putative self-recognition faces are approximately orthogonal to each other in Fig. 4. This is consistent with a self-association model in which four cyclotide molecules come together, with the activity-influencing hydrophilic surfaces facing inward and the hydrophobic surfaces oriented together on one face of the tetramer (Fig. 5). Such a reversible oligomerization could improve the absorption and dispersion of cyclotides in biological systems by allowing both the solubility of monomers in aqueous environments and of oligomers in the membrane, switching the effective hydrophobicity of the peptides.

The dramatic effect of the loss of structural rigidity on bioactivity seen in mutants E7A and G12A is also consistent with a

FIGURE 4. **Localization of residues critical for hemolytic and insecticidal activity of kalata B1 and the hydrophobic patch of kalata B1.** The figures on the *right* are rotated 180° relative to those on the *left*. *a*, mutated residues giving <20% hemolysis at 60 μM peptide concentration are shown in *red*. The wild-type peptide displays 69% hemolysis at this concentration. Functionally essential residues without concomitant structural perturbation are seen to cluster on one face of the molecule around E7. *b*, the surface position of residues critical for insecticidal activity. Mutated residues giving <70% insecticidal activity at 230 ppm are shown in *orange*, relative to the wild-type peptide normalized to 100% activity. *c*, the hydrophobic residues of kalata B1 are highlighted in *green*, showing a dominant hydrophobic patch on the lower section of the framework. *d*, membrane penetrating residues as measured by NMR shown in *dark blue* (42), showing a correspondence with the dominant hydrophobic surface patch.

self-association mechanism, where the conformation of the peptide that is capable of self-recognition is thrown into dynamic equilibrium with other conformations. In a tetramer dependent on multiple self-recognition interfaces any reduction in the average lifetime of each self-association face would have a multiplicative effect on the lifetime of the entire oligomer. Mutants that displayed a loss of structural rigidity as judged by NMR (E7A and G12A) displayed a dramatic loss of bioactivity. This is consistent with the reduced rigidity and total loss of activity in a series of acyclic permutants (46) and capped acyclic permutants (47).

Analysis of the stability of two inactive mutants was undertaken to determine if the resilience of the scaffold could be retained while eliminating activities that would be undesirable in pharmaceutical applications. Two mutants on loop 1 were selected, G6A because of the presumably steric nature of its interference with activity and E7A because of the possible structural contribution of this residue in the wild-type peptide. Mutant G6A was found to display similar resistance to proteolytic and thermal degradation and to extremes of pH as the wild-type peptide, consistent with a precise steric clash removing hemolytic activity in this mutant. Mutant E7A was also found to have comparable resistance to the wild-type peptide, indicating that the cyclic backbone and cystine knot alone are sufficient structural features to confer extreme stability. The resilience of both inactive mutants strengthens the potential of the cyclotide framework for stabilization of bioactive peptide epitopes for therapeutic applications.

Previously, it has been reported that the divalent cation Mn^{2+} binds to kalata B1 (41). The presence of a metal binding site may be functionally significant, because it may facilitate the interaction of kalata B1 (and other cyclotides) to membrane surfaces, particularly anionic membrane surfaces (42). A representative group of mutants, which were selected based on their activity and the presence/absence of a carboxyl group, were tested for Mn^{2+} binding and compared with kalata B1. Kalata B1 and the two carboxyl-containing mutants, T16A (an inactive mutant) and T27A (an active mutant), showed very similar responses to Mn^{2+}. Significant broadening of the amide signals from loop 1 and complete broadening of the amide signals from loop 3 was observed, which is consistent with previous reports and identifies the metal binding face of kalata B1 (42). At similar concentrations of peptide and Mn^{2+}, the amide signals around the corresponding region for E7A showed significantly less broadening, confirming that the carboxyl of Glu-7 is responsible for metal binding. This finding is consistent with the fact that carboxyl groups have been reported to coordinate Mn^{2+} binding in proteins (51); removal of the carboxyl in the E7A mutant quenches the binding. Because the inactive mutant T16A binds Mn^{2+}, it appears that metal binding may not be an important factor for the activity of the cyclotides.

The current study has clearly shown that the cyclotide framework can accommodate sequence variations and maintain a well defined structure with the native fold. Given this conservation of the overall fold in the kalata B1 mutants, it appears likely that it is the side chains that have a greater role in maintaining the activity of the cyclotides. Such a scenario has also been observed for other disulfide-rich peptides such as the α-conotoxins where the native α-helical fold is maintained despite the sequence diversity throughout the family, but the selectivity and specificity for the nicotinic acetylcholine receptor varies enormously based on the side chains that are available to interact with the receptor subunits (52, 53).

In conclusion, significant advances have been made in the understanding of the adaptability of the cyclotide framework to modifications. Selected mutants lacking undesirable hemolytic activity were found to retain the characteristic stability of the framework, verifying its suitability for pharmacological applications. The conserved hydrogen-bonding network of the loop 1 glutamate to loop 3 was found to play a critical functional role, and the activity of kalata B1 was found to depend on a surface patch of predominantly hydrophilic residues. This information will be valuable in future experiments aimed at exploiting the cyclic cystine knot scaffold in drug design applications.

REFERENCES

1. Gran, L. (1970) *Medd. Nor. Farm. Selsk.* **12,** 173–180
2. Saether, O., Craik, D. J., Campbell, I. D., Sletten, K., Juul, J., and Norman, D. G. (1995) *Biochemistry* **34,** 4147–4158
3. Craik, D. J., Daly, N. L., Bond, T., and Waine, C. (1999) *J. Mol. Biol.* **294,** 1327–1336
4. Gustafson, K. R., Sowder, R. C., 2nd, Henderson, L. E., Parsons, I. C., Kashman, Y., Cardellina, J. H., 2nd, McMahon, J. B., Buckheit R.W., Pannell, L. K., and Boyd, M. R. (1994) *J. Am. Chem. Soc.* **116,** 9337–9338
5. Witherup, K. M., Bogusky, M. J., Anderson, P. S., Ramjit, H., Ransom, R. W., Wood, T., and Sardana, M. (1994) *J. Nat. Prod.* **57,** 1619–1625
6. Schopke, T., Hasan Agha, M. I., Kraft, R., Otto, A., and Hiller, K. (1993) *Sci. Pharm.* **61,** 145–153
7. Broussalis, A. M., Goransson, U., Coussio, J. D., Ferraro, G., Martino, V., and Claeson, P. (2001) *Phytochemistry* **58,** 47–51
8. Trabi, M., and Craik, D. J. (2004) *Plant Cell* **16,** 2204–2216
9. Simonsen, S. M., Sando, L., Ireland, D. C., Colgrave, M. L., Bharathi, R., Goransson, U., and Craik, D. J. (2005) *Plant Cell* **17,** 3176–3189
10. Trabi, M., and Craik, D. J. (2002) *Trends Biochem. Sci.* **27,** 132–138
11. Craik, D. J. (2006) *Science* **311,** 1563–1564
12. Gran, L., Sandberg, F., and Sletten, K. (2000) *J. Ethnopharmacol.* **70,** 197–203
13. Bokesch, H. R., Pannell, L. K., Cochran, P. K., Sowder, R. C., 2nd, McKee, T. C., and Boyd, M. R. (2001) *J. Nat. Prod.* **64,** 249–250
14. Tam, J. P., Lu, Y. A., Yang, J. L., and Chiu, K. W. (1999) *Proc. Natl. Acad. Sci. U. S. A.* **96,** 8913–8918
15. Lindholm, P., Goransson, U., Johansson, S., Claeson, P., Gullbo, J., Larsson, R., Bohlin, L., and Backlund, A. (2002) *Mol. Cancer Ther.* **1,** 365–369
16. Goransson, U., Sjogren, M., Svangard, E., Claeson, P., and Bohlin, L. (2004) *J. Nat. Prod.* **67,** 1287–1290
17. Jennings, C., West, J., Waine, C., Craik, D., and Anderson, M. (2001) *Proc. Natl. Acad. Sci. U. S. A.* **98,** 10614–10619
18. Kamimori, H., Hall, K., Craik, D. J., and Aguilar, M. I. (2005) *Anal. Biochem.* **337,** 149–153
19. Svangard, E., Burman, R., Gunasekera, S., Lovborg, H., Gullbo, J., and Goransson, U. (2007) *J. Nat. Prod.* **70,** 643–647
20. Nourse, A., Trabi, M., Daly, N. L., and Craik, D. J. (2004) *J. Biol. Chem.* **279,** 562–570
21. Nair, S. S., Romanuka, J., Billeter, M., Skjeldal, L., Emmett, M. R., Nilsson, C. L., and Marshall, A. G. (2006) *Biochim. Biophys. Acta* **1764,** 1568–1576
22. Jennings, C. V., Rosengren, K. J., Daly, N. L., Plan, M., Stevens, J., Scanlon, M. J., Waine, C., Norman, D. G., Anderson, M. A., and Craik, D. J. (2005) *Biochemistry* **44,** 851–860
23. Colgrave, M. L., and Craik, D. J. (2004) *Biochemistry* **43,** 5965–5975
24. Craik, D. J., Simonsen, S., and Daly, N. L. (2002) *Curr. Opin. Drug Discov. Dev.* **5,** 251–260
25. Hernandez, J. F., Gagnon, J., Chiche, L., Nguyen, T. M., Andrieu, J. P., Heitz, A., Trinh Hong, T., Pham, T. T., and Le Nguyen, D. (2000) *Biochem-*

istry **39,** 5722–5730
26. Craik, D. J., Daly, N. L., and Waine, C. (2001) *Toxicon* **39,** 43–60
27. Kimura, R. H., Tran, A. T., and Camarero, J. A. (2006) *Angew. Chem. Int. Ed. Engl.* **45,** 973–976
28. Rosengren, K. J., Daly, N. L., Plan, M. R., Waine, C., and Craik, D. J. (2003) *J. Biol. Chem.* **278,** 8606–8616
29. Schnolzer, M., Alewood, P., Jones, A., Alewood, D., and Kent, S. B. (1992) *Int. J. Pept. Protein Res.* **40,** 180–193
30. Tam, J. P., and Lu, Y. A. (1997) *Tetrahedron Lett.* **38,** 5599–5602
31. Guntert, P., Mumenthaler, C., and Wuthrich, K. (1997) *J. Mol. Biol.* **273,** 283–298
32. Brunger, A. T., Adams, P. D., and Rice, L. M. (1997) *Structure* **5,** 325–336
33. Rice, L. M., and Brunger, A. T. (1994) *Proteins* **19,** 277–290
34. Stein, E. G., Rice, L. M., and Brunger, A. T. (1997) *J. Magn. Reson.* **124,** 154–164
35. Linge, J. P., and Nilges, M. (1999) *J. Biomol. NMR* **13,** 51–59
36. Hutchinson, E. G., and Thornton, J. M. (1996) *Protein Sci.* **5,** 212–220
37. Laskowski, R. A., Rullmannn, J. A., MacArthur, M. W., Kaptein, R., and Thornton, J. M. (1996) *J. Biomol. NMR* **8,** 477–486
38. Daly, N. L., Love, S., Alewood, P. F., and Craik, D. J. (1999) *Biochemistry* **38,** 10606–10614
39. Dawson, P. E., Muir, T. W., Clark-Lewis, I., and Kent, S. B. (1994) *Science* **266,** 776–779
40. Wishart, D. S., Sykes, B. D., and Richards, F. M. (1991) *J. Mol. Biol.* **222,** 311–333
41. Skjeldal, L., Gran, L., Sletten, K., and Volkman, B. F. (2002) *Arch. Biochem. Biophys.* **399,** 142–148
42. Shenkarev, Z. O., Nadezhdin, K. D., Sobol, V. A., Sobol, A. G., Skjeldal, L., and Arseniev, A. S. (2006) *FEBS Lett.* **273,** 2658–2672
43. Tam, J. P., and Lu, Y. A. (1998) *Protein Sci.* **7,** 1583–1592
44. Mulvenna, J. P., Wang, C., and Craik, D. J. (2006) *Nucleic Acids Res.* **34,** D192–D194
45. Plan, M. R., Goransson, U., Clark, R. J., Daly, N. L., Colgrave, M. L., and Craik, D. J. (2007) *Chembiochem* **8,** 1001–1011
46. Daly, N. L., and Craik, D. J. (2000) *J. Biol. Chem.* **275,** 19068–19075
47. Simonsen, S. M., Daly, N. L., and Craik, D. J. (2004) *FEBS Lett.* **577,** 399–402
48. Herrmann, A., Svangard, E., Claeson, P., Gullbo, J., Bohlin, L., and Goransson, U. (2006) *Cell Mol. Life Sci.* **63,** 235–245
49. Shai, Y. (1999) *Biochim. Biophys. Acta* **1462,** 55–70
50. Ojcius, D. M., and Young, J. D. (1991) *Trends Biochem. Sci.* **16,** 225–229
51. Ghirardi, M. L., Lutton, T. W., and Seibert, M. (1998) *Biochemistry* **37,** 13559–13566
52. Millard, E. L., Daly, N. L., and Craik, D. J. (2004) *Eur. J. Biochem.* **271,** 2320–2326
53. McIntosh, J. M., Gardner, S., Luo, S., Garrett, J. E., and Yoshikami, D. (2000) *Eur. J. Pharmacol.* **393,** 205–208

Fig. S1. Attenuation by Mn^{2+} of intensities of selected cross-peaks (HN-Hα) in TOCSY spectra for various mutants and kalata B1. Relative peak intensities after the addition of Mn^{2+} are shown for kalata B1 (kB1), T27A, T16A and E7A. The sequence of kalata B1 is shown at the bottom of the panel with each loop labelled. The black arrows highlight regions that have been significantly broadened.

Supplementary Figure 1

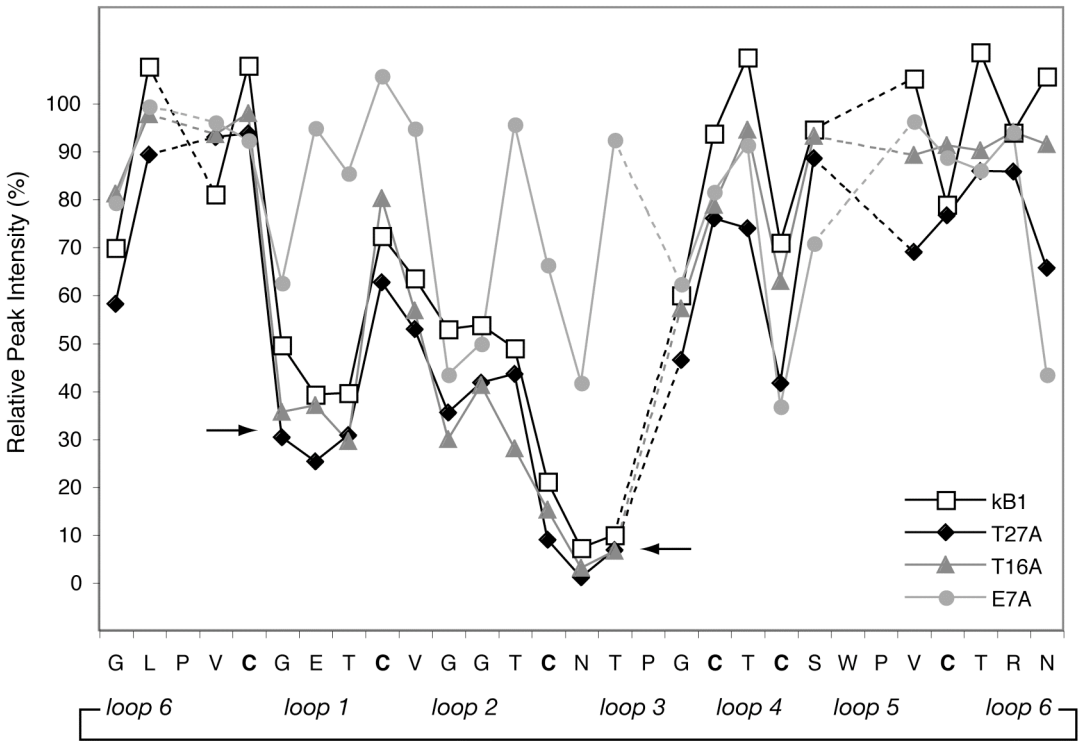

Alanine Scanning Mutagenesis of the Prototypic Cyclotide Reveals a Cluster of Residues Essential for Bioactivity

Shane M. Simonsen, Lillian Sando, K. Johan Rosengren, Conan K. Wang, Michelle L. Colgrave, Norelle L. Daly and David J. Craik

J. Biol. Chem. 2008, 283:9805-9813.
doi: 10.1074/jbc.M709303200 originally published online February 7, 2008
